PERGAMON

Journal of Structural Geology 23 (2001) 609–617

JOURNAL OF STRUCTURAL GEOLOGY

www.elsevier.nl/locate/jstrugeo

Rotation of rigid elliptical cylinders in viscous simple shear flow: analogue experiments

F.O. Marques*, S. Coelho

LATTEX, Fac. Ciências, Universidade de Lisboa, Edifício C2, Piso 5, 1749-016 Lisboa, Portugal

Received 15 September 1999; accepted 19 July 2000

Abstract

We used experiments to investigate the behaviour of rigid elliptical cylinders embedded in a viscous fluid of finite thickness, and for very small ratios (S) between shear zone width (z) and the shortest principal axis (e_2) of the ellipse that constitutes the base of the elliptical cylinder ($3.5 \geq S = z/e_2 \geq 1.2$). Former theoretical and experimental work on the rotation of rigid inclusions immersed in a viscous matrix considered infinite shear zone thickness and/or a very large ratio between shear zone thickness and inclusion size ($S >> 1$), and concluded that inclusions rotate continuously and synthetically with the applied bulk simple shear flow (except for inclusions with infinite axial ratio). Our results depart greatly from the analytical predictions. Experiments were carried out at constant shear zone thickness, but variable S and degree of coupling at the inclusion/matrix interface. The results show that: (1) confined inclusion rotation always deviates from theoretical predictions for infinite shear zone thickness, even for synthetic rotation; (2) the deviation in the angular velocity and/or in the sense of rotation increases as S approaches 1, and antithetic rotation is possible from a position with ellipse longest axis parallel to the shear plane; and (3) a slipping inclusion/matrix interface greatly enhances deviation from theoretical predictions, with antithetic rotations to as much as 20°.

1. Introduction

Previous analytical work has dealt with the rotation of rigid inclusions immersed in a viscous matrix of infinite thickness subject to simple shear (e.g., Jeffery, 1922; Bretherton, 1962; Freeman, 1985; Ghosh and Ramberg, 1976). Substantiating their analytical results, experimental work by Ghosh and Ramberg (1976) used very small inclusions relative to the thickness of the viscous matrix. The result is that, under these conditions, the inclusions rotate continuously and synthetically with the applied simple shear flow.

According to Ghosh and Ramberg (1976), the amount of rotation of elliptical rigid inclusions is controlled by the inclusion axial ratio (R), its initial orientation (ϕ) and the relative amount of pure and simple shear (S_r). Because our experimental work considered only simple shear, we are only concerned with the results of Ghosh and Ramberg (1976) for $Sr = 0$ ($Sr = 1$ is coaxial flow). For simple shear flow, all inclusions rotate continuously and synthetically with the applied bulk simple shear; the limit case are inclusions with infinite axial ratio, which act as passive markers and tend to a stable position with the longest axis parallel to the shear plane and shear direction. Thus, if the initial position coincides with the stability plane, the material line does not rotate at all.

To our knowledge, with the exception of Ildefonse and Mancktelow (1993) and Marques and Cobbold (1995), published experimental work assumed a non-slipping interface between inclusions and surrounding matrix. In this case, there is no velocity discontinuity across the inclusion/matrix boundary. Ildefonse and Mancktelow (1993) argued that in natural systems this assumption is not always true (e.g. pressure shadows around rigid objects, mantle-core structures in porphyroclast systems) and they developed an experiment to quantify the effect of a slipping interface on the inclusion's rotation. A slipping interface induces a slower rotation and the inclusion tends to stabilise with its longest axis parallel to the shear plane (Ildefonse and Mancktelow, 1993).

Marques and Cobbold (1995) verified that no rotation, or even antithetic rotation of ellipsoidal inclusions with their longest axes initially parallel to the shear plane and shear direction, are possible in bulk simple shear flow. The ellipsoidal inclusions had axial ratios between 2.2 and 3.6. According to Ghosh and Ramberg (1976) inclusions should have rotated continuously and synthetically with the applied

* Corresponding author.
E-mail address: fmarques@fc.ul.pt (F.O. Marques).

0191-8141/01/$ - see front matter
PII: S0191-8141(00)00135-8

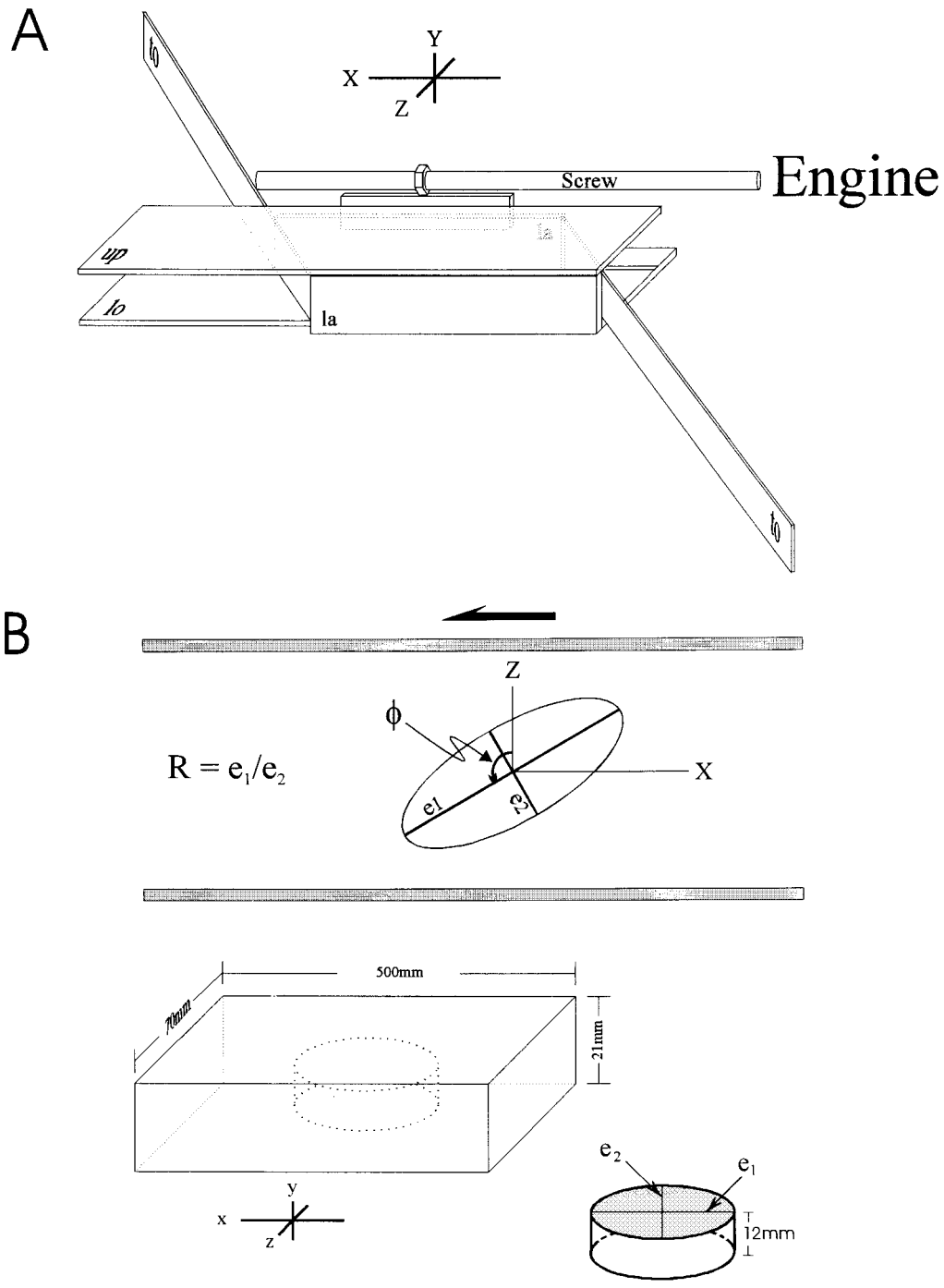

Fig. 1. (A) Schematic representation of the simple shear box used in the experiments. up—upper wall; lo—lower wall; la—lateral walls; to—top walls. X, Y and Z are kinematic axes. (B) Schematic representation of the model with the inclusion. x, y and z are principal dimensions of the model. e_1 and e_2 are principal axis of the elliptical cylinder.

simple shear flow. The major difference between the experiments of Ghosh and Ramberg (1976) and those of Marques and Cobbold (1995) is the ratio of shear zone thickness over inclusion. Ghosh and Ramberg (1976) considered infinite width shear zones or large shear zone thickness/inclusion ratios, whereas Marques and Cobbold (1995) used a finite shear zone (shear box width = 50mm) and large ellipsoidal inclusions relative to the rig width.

Strain localization is commonly observed in mylonites in the form of shear bands of variable thickness. Layers of different viscosity flow at different velocities, with generation of microscopic/mesoscopic shear zones in which the ratio between their thickness and porphyroclast/inclusion dimension can approach one. The aim of the present work is to study the influence of shear zone thickness on the behaviour of rigid inclusions immersed in a viscous fluid

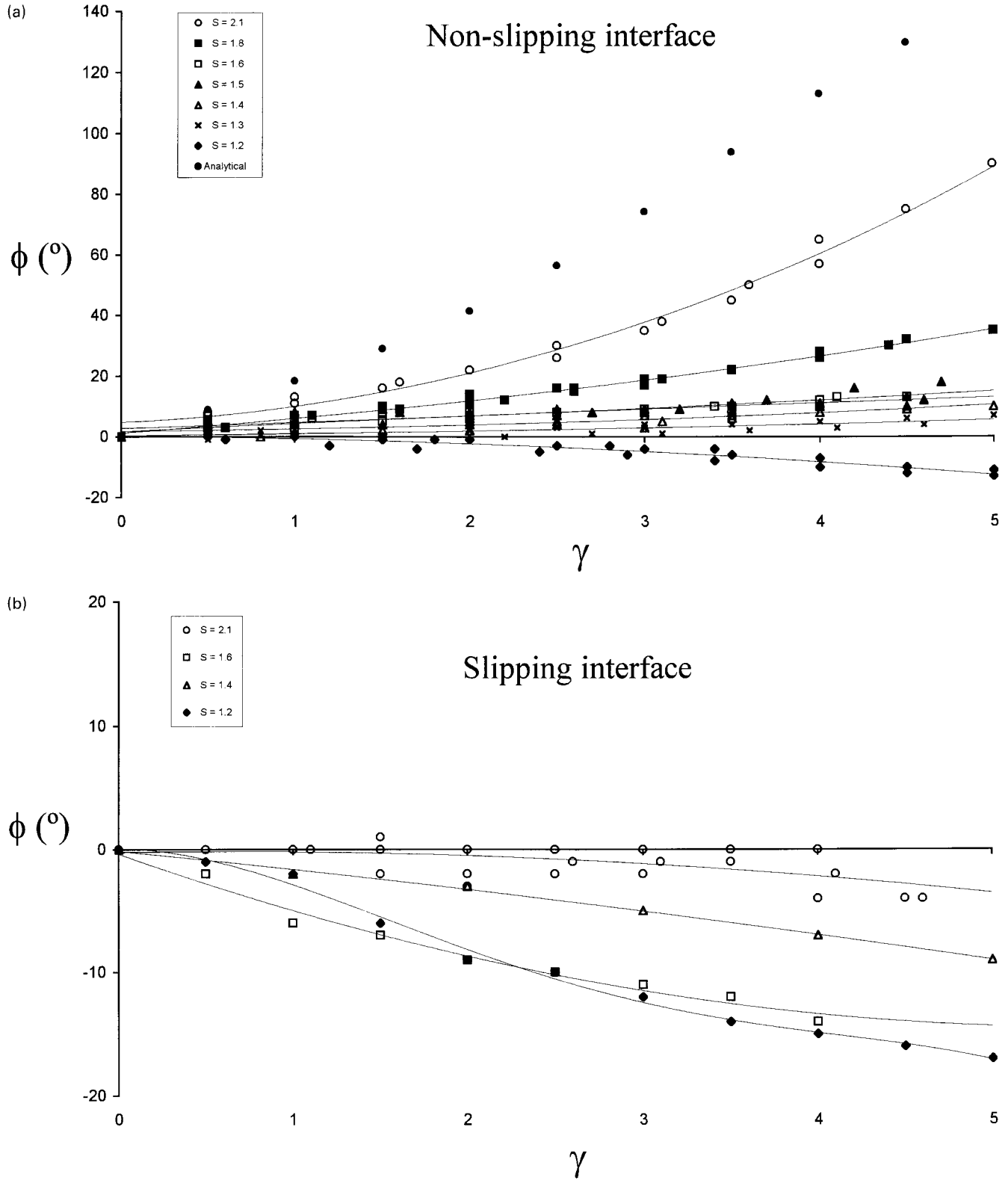

Fig. 2. Graphs of results for: (A) Non-slipping inclusion/matrix interface, and (B) Slipping inclusion/matrix interface. Compare experimental results in A and B with analytical result in A ($S = \infty$).

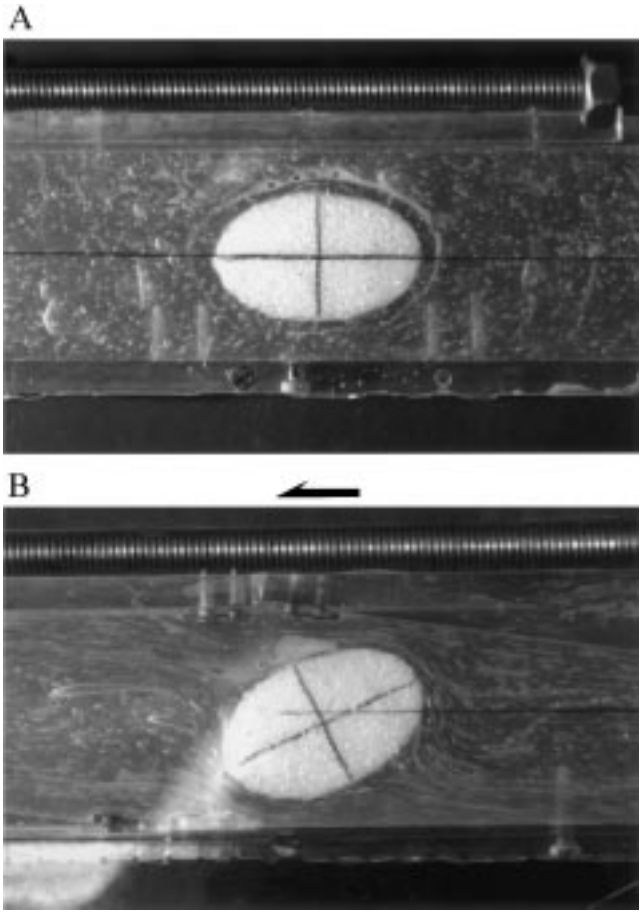

Fig. 3. Experimental results for $S \cong 1.6$ and a non-slipping inclusion/matrix interface. (A) initial state; (B) final state, $\gamma \cong 4.0$. Note that the inclusion has rotated little synthetically when compared with the analytical prediction (cf. Fig. 2A). Top to the left shear. Plane of photo is xz.

subject to bulk simple shear flow ($S_r = 0$), and analyse deviations from what is analytically predicted for infinite shear zone thickness. Instead of large shear zone thickness/inclusion ratios and/or non-slipping interfaces as used by former authors, we worked with very small ratios (S) between shear zone width (z) and ellipse shortest principal axis (e_2) ($3.5 > S = z/e_2 > 1.2$), and a variable degree of coupling at the interface.

2. Experimental procedure

The analogue materials used are transparent silicone putty (a polydimethyl-siloxane-PDMS-manufactured by Dow Corning of Great Britain under the trade name SGM 36), as the ductile matrix (see Weijermars 1986a,b,c for PDMS properties), and a rigid plastic material with density similar to the PDMS for the inclusions.

The experiments were carried out in a Perspex simple shear rig capable of shear strains (γ) up to 12, with the shear plane vertical. The shear box (Fig. 1A) is comprised of two horizontal fixed upper and lower walls (normal to the shear plane), two vertical side walls (parallel to the shear plane-*XY*), one fixed and the other driven by a motor (these transmit simple shear flow to PDMS), and two vertical top walls articulated with the side walls to keep the volume constant and maintain geometry of the model. Undesirable boundary effects resulting from the approximation of the two top walls can only arise at shear strain values higher than the ones used in our experiments. The model dimensions (x, y and z in Fig. 1B) were $500 \times 21 \times 70$mm. To assure homogeneous simple shear flow in the model, PDMS adheres perfectly to the lateral walls, and a neutral

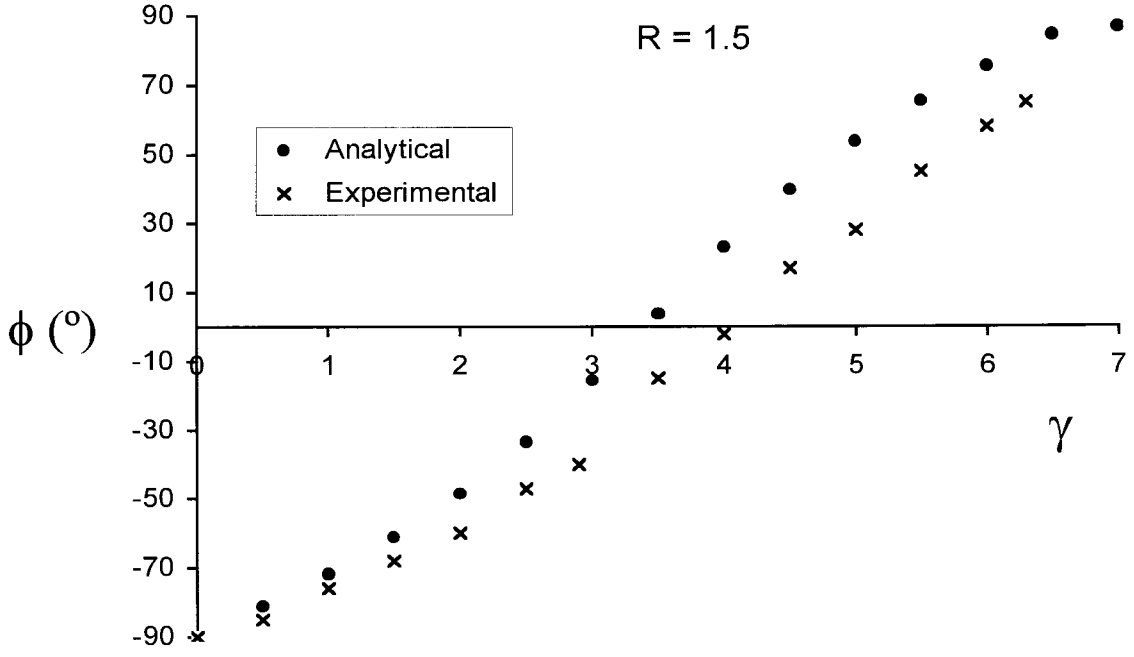

Fig. 4. Comparison between analytical predictions (Ghosh and Ramberg, 1976) and experimental results for the same value of ellipse axial ratio ($R \cong 1.5$).

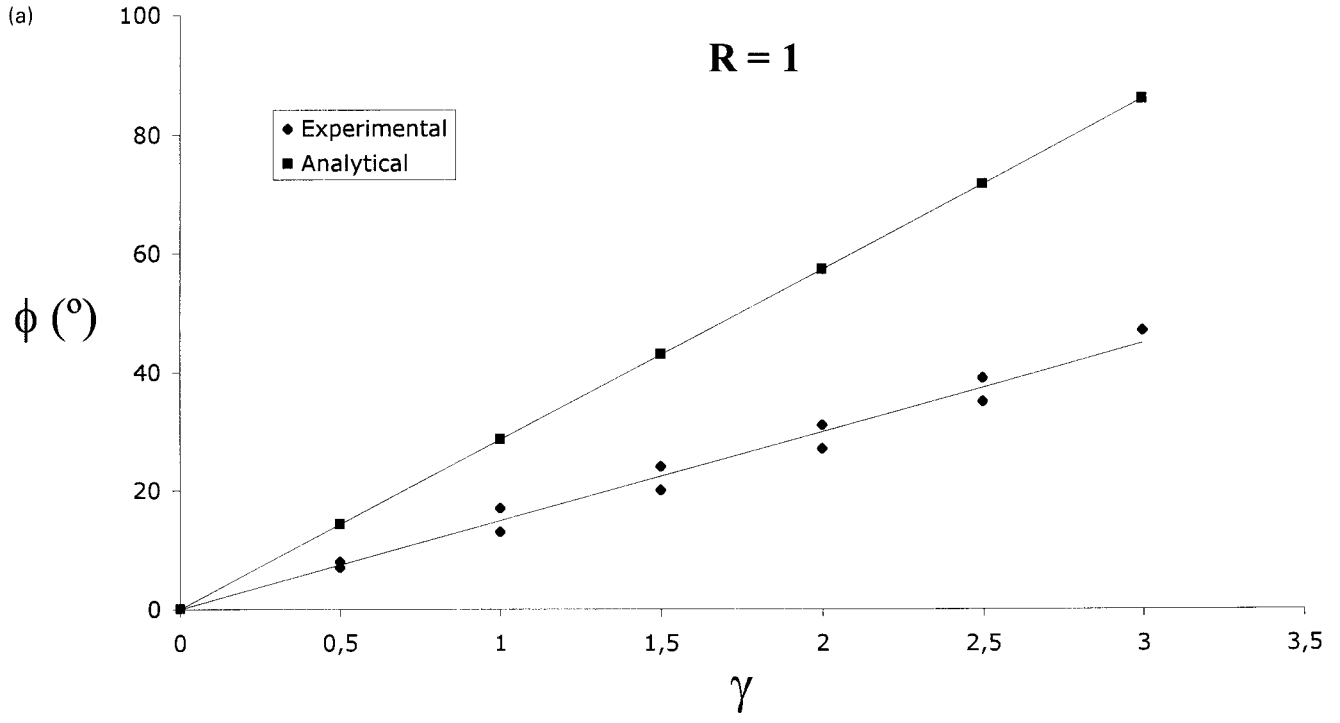

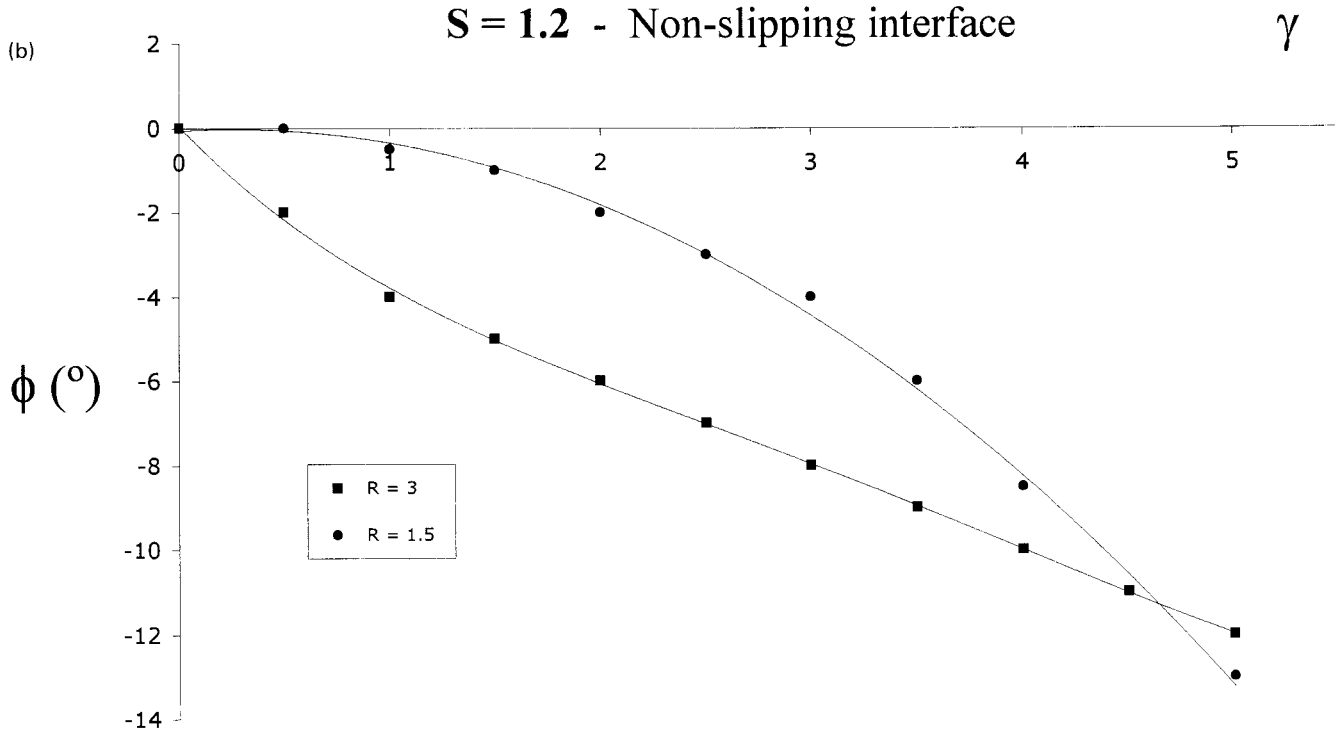

Fig. 5. (A) Graph of the results for $R \cong 1$, $S \cong 1.2$ and a non-slipping matrix/inclusion interface; the analytical curve is also included for comparison. (B) Graphical representation of the results for $R \cong 3$, $R \cong 1.5$, $S \cong 1.2$ and a non-slipping inclusion/matrix interface.

liquid soap was used to assure that friction was kept to a minimum on all other walls. In this way, simple shear flow is only driven by the lateral walls.

The rigid inclusions (Fig. 1B) had an elliptical section, and for most experiments an identical axial ratio of *ca.* 1.5 ($R = e_1/e_2$). The shape of the inclusion (Fig. 1B) was chosen to allow comparison with the 2-D analytical results of Ghosh and Ramberg (1976). The variable that most influences the rotation of rigid inclusions in a confined environment is the ratio (S) between shear zone width (z)

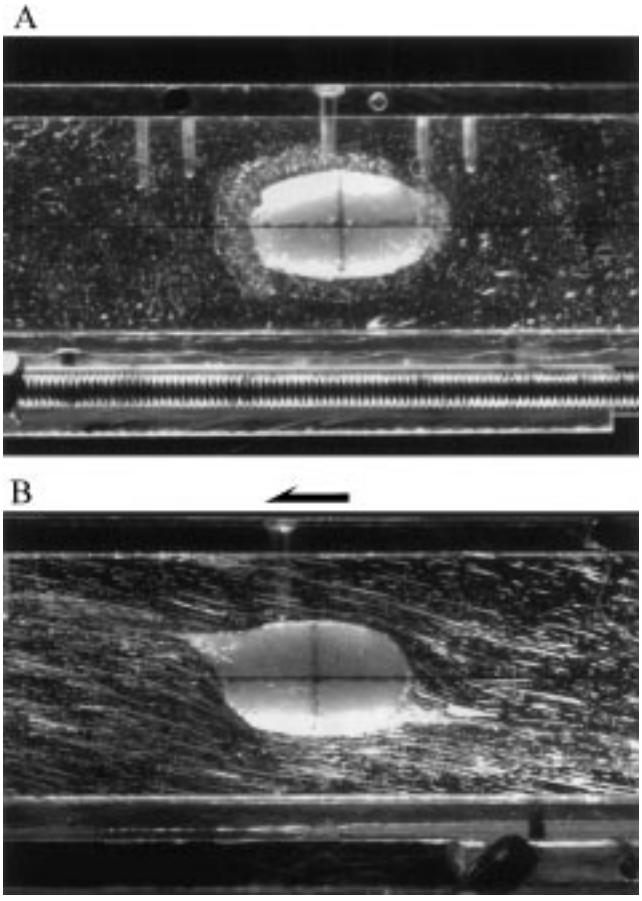

Fig. 6. Experimental results for $S \cong 2.1$ and a slipping inclusion/matrix interface. (A) initial state; (B) final state, $\gamma \cong 4.0$. Note that the inclusion has virtually not rotated up to $\gamma \cong 4.0$. Top to the left shear. Plane of photo is xz.

and shortest principal axis (e_2) of the ellipse that constitutes the base of the elliptical cylinder (see Fig. 1); $S = z/e_2$ and varies between ∞ and 1. We used seven rigid inclusions with e_2 values of 33, 40, 43, 47, 50, 53 and 57 mm, which correspond, respectively, to S values of 2.1, 1.8, 1.6, 1.5, 1.4, 1.3 and 1.2 because $z \cong 70$ mm. An $e_2 \cong 20$ mm ellipse was also used in order to allow comparisons with the results of Ghosh and Ramberg (1976), because then $S \cong 3.5$, which can be considered large. For testing purposes, we also performed two other experiments, one with a cylinder ($R \cong 1$) and the other with an elliptical cylinder ($R \cong 3$). The rigid inclusions were always put inside the PDMS matrix with their e_1e_2 plane normal to the shear plane and e_1 axis parallel to the shear direction (X).

According to the slipping or non-slipping nature of the inclusion/matrix boundary, two sets of experiments were performed, both with the same above described initial conditions. In the first set of experiments the interface was non-slipping, by placing the inclusion directly in contact with the PDMS matrix. In the second set, the inclusion surface was covered with a film of lubricant, before its immersion in the PDMS, to make the inclusion/matrix boundary slipping.

The angle ϕ measured between the normal to the shear plane and the major axis of the elliptical inclusion (e_1) was considered positive when rotation was synthetic (top to the left shear and anticlockwise rotation of the inclusion in our experiments) and negative when rotation was antithetic (top to the left shear and clockwise rotation of the inclusion in our experiments).

The shear strain rate in the presented experiments was constant and approximately equal to $10^{-3}\ s^{-1}$. We tested the influence of strain rate variation on the rotation of the elliptical cylinders, but the results were not conclusive because they were not significantly different, even up to shear strain rate geologically unrealistic ($0.5\ s^{-1}$).

3. Results

For each experiment, we plotted all the data in a spreadsheet capable of producing graphs with different trendlines. The procedure used by the software is the least squares method and, with the exception of one experiment, the best-fit for all data sets are polynomial with a degree of fitness greater than 0.9 (where 1.0 is perfect correlation).

3.1. Experiments with a non-slipping interface

The results of the experiments with $R \cong 1.5$ are represented in the graphs of Fig. 2a and a representative example on the photo of Fig. 3. The deviations from theoretical predictions are clear from the graphs: in the experiments all inclusions except one rotated synthetically, but with less magnitude and at slower angular velocities then theoretically predicted for $S = \infty$; for $S < 1.3$ antithetic rotation occurred (Fig. 2a).

Fig. 4 shows the experimental results of $S \cong 3.5$ in comparison with the theoretical prediction for $S = \infty$ and an identical R value. The graphs show that the inclusion rotates synthetically, but still significantly deviates from the analytical solution of Ghosh and Ramberg (1976). Thus, at an S value as large as 3.5, the flow is still sufficiently disturbed by the inclusion.

Following the results of the experiments with constant R and variable S, we performed two other complementary experiments in which S was constant and R variable. Results for $R \cong 1$ and $R \cong 3$ with $S \cong 1.2$ are represented in Fig. 5a and b respectively. The graph of Fig. 5b shows that the cylinder rotates significantly slower than what is theoretically predicted for $S = \infty$ and $R = 1$. The graph of Fig. 5b shows that both elliptical cylinders rotate antithetically, and that the rotation of the two inclusions follow different paths to an identical orientation at $\gamma \cong 5$.

3.2. Experiments with a slipping interface

The results of these experiments are graphically represented in Fig. 2b, and the images of the most representative results

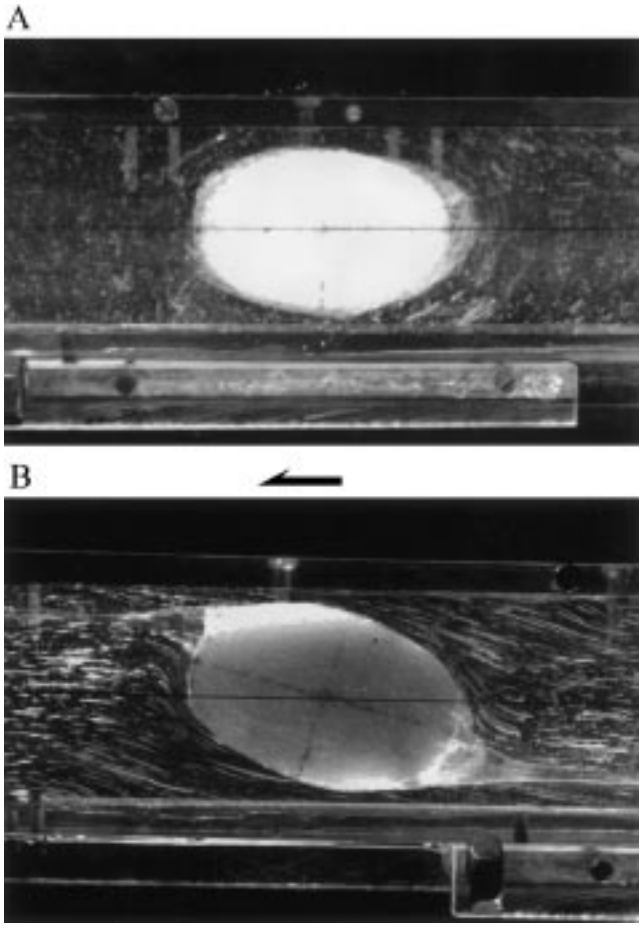

Fig. 7. Experimental results for $S \cong 1.2$ and a slipping inclusion/matrix interface. (A) initial state; (B) final state, $\gamma \cong 4.0$. Note that the inclusion has significantly rotated clockwise, which is antithetic with the applied shear. Top to the left shear. Plane of photo is xz.

in Figs. 6 and 7. As in the first set of experiments, deviations from theoretical predictions for $S = \infty$ are significant, and even greater than for non-slipping inclusion/matrix interface (Fig. 8a and b), and antithetic rotation occurs for $S \leq 2.1$. The major differences between experiments with non-slipping or slipping boundaries lie in the angular velocity and amount of synthetic and antithetic rotation, and the S value at which antithetic rotation starts to occur. Slipping inclusion/matrix boundaries induce reduction of the amount of synthetic rotation and angular velocity, and increase of the amount of antithetic rotation and angular velocity, when compared with the behaviour of inclusions with non-slipping boundaries.

From the graphs we can also deduce that, for each set of experiments, there is an S value at which there should be no rotation of the inclusion at all. In fact, the inclusion with $S \cong 2.1$ rotated very little up to $\gamma \cong 4.0$, as shown in Fig. 8a and Fig. 6.

4. Discussion

As in Marques and Cobbold (1995), we believe that the peculiar behaviour displayed by our experiments is a direct consequence of the geometrical confinement, which leads to a squeezing of the flow between the inclusion and the shear walls. Close to the inclusion, the laminar flow is strongly disturbed by the object interference (obstacle to matrix flow).

Fig. 9 shows that, close to the inclusion, the silicone matrix can be divided into four quadrants in the shape of wedges; these straighten towards the middle part of the inclusion, *i.e.*, from *a* (thicker) to *b* (thinner) in Fig. 9A. This means that when the walls move to produce simple shear flow, the silicone matrix is driven into the thinner part of the wedges in quadrants 1 and 3 (from *a* to *b* in Fig. 9A), and the opposite happens in the other two quadrants (Q_2 and Q_4). Because silicone is a viscous fluid, it has great difficulty in going through the thinner section in *a*, and pressure increases in Q_1 and Q_3 (*P* in Fig. 9A). The opposite happens in Q_2 and Q_4, where silicone is driven from a narrower section towards a wider section; then pressure decreases (*p* in Fig. 9A) because insufficient silicone goes through *a*. This *wedge effect* induces higher normal pressure on the surface of the inclusion in Q_1 and Q_3, and lower normal pressure in Q_2 and Q_4. This results in a torque that makes the inclusion rotate clockwise in response to a top to the left shear flow (antithetic rotation).

As a result of this antithetic rotation, the areas of Q_1 and Q_3 increase and the areas of Q_2 and Q_4 decrease (respectively *A* and *a* in Fig. 9B); this means that the inclusion's antithetic rotation tends to reduce the pressure gradient induced by the wedge effect in consecutive quadrants (Q_1 and Q_2, and Q_3 and Q_4). For each increment of shear flow, normal pressure increases in Q_1 and Q_3 (conversely decreases in Q_2 and Q_4), the inclusion rotates antithetically and pressure decreases in those quadrants (increases in the other two) as a result of area increase (decrease in Q_2 and Q_4).

To significantly disturb the typical rotation of an elliptical inclusion (for $S = \infty$), pressure-gradient-driven rotation (which is antithetic) must overcome viscous-flow-driven rotation (or vorticity-induced rotation, which is synthetic). Then, it is more difficult to disturb the inclusion rotation when the inclusion/matrix interface is non-slipping (greater viscous-flow-driven rotation) than when it is slipping (smaller viscous-flow-driven rotation). When the *S* value increases, the pressure induced by the wedge effect decreases, and thus viscous-flow-driven rotation dominates and particle rotates synthetically. Conversely, when *S* is small (approaches 1), the wedge effect and pressure-gradient-driven rotation dominate and strongly influence the inclusion's rotation. If the sum of viscous-flow-driven rotation and pressure-gradient-driven rotation is positive, the rotation is synthetic; if negative, the rotation is antithetic.

During progressive deformation of the PDMS model, the lubricant (originally with a uniform distribution at the

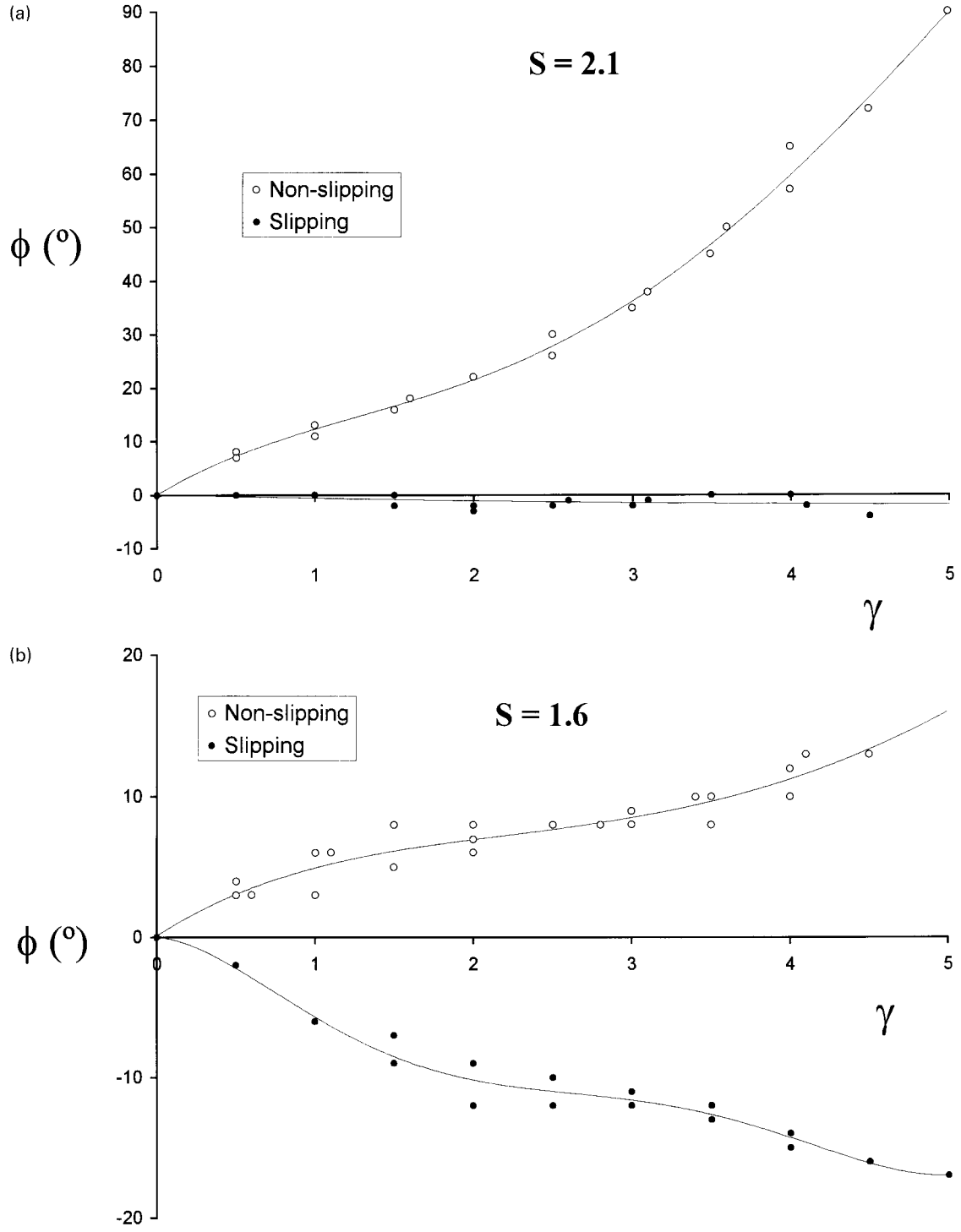

Fig. 8. Comparisons between the most contrasting results from experiments with non-slipping and slipping inclusion/matrix interface. (a) for $S \cong 2.1$ and (b) for $S \cong 1.6$.

matrix/inclusion interface) migrated from the areas exposed to maximum tension to minimum tension areas, and such accumulations are interpreted as pressure shadows. Their stair-stepping geometry resembles the σ-type core-mantle structures of Passchier and Simpson (1986) and can be used as a kinematic indicator, as shown by our results (Figs. 6 and 7). Despite the similarity, these structures have a different origin, because they do not result from dynamic recrystallisation of the inclusion, but from fluid migration to zones of low pressure. The asymmetric geometry of pressure shadows develops because the inclusion rotates a small amount and/or stabilises with the longest axis at a small

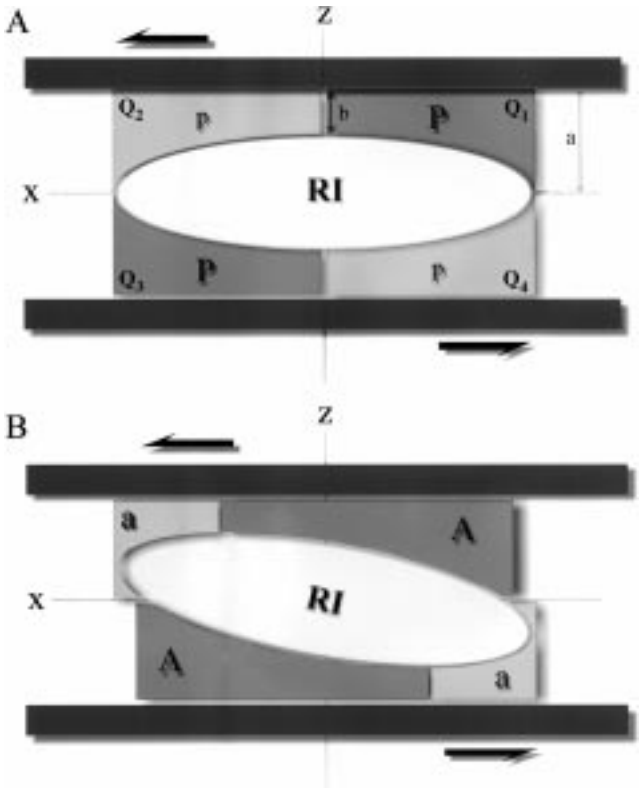

Fig. 9. Sketch to illustrate antithetic rotation of the rigid inclusion (RI). Shear flow drives the silicone matrix into the wedge that straightens from *a* to *b*, and the opposite happens in the other two quadrants. In quadrants 1 and 3 (Q_1 and Q_3) pressure is higher (P) than in quadrants 2 and 4 (p in Q_2 and Q_4). If the inclusion rotates antithetically, the areas of Q_1 and Q_3 increase (A) and the areas of Q_2 and Q_4 decrease (a), reducing the pressure gradient between Q_1 and Q_2, and Q_3 and Q_4.

angle to the shear plane. Therefore, this geometry is stable, not transient.

5. Conclusions

Previous analytical and experimental results on the rotation of rigid inclusions in a viscous matrix are valid only for infinite width shear zones or large *S* values. Our experiments show that the behaviour of inclusions is significantly different when *S* is small.

Deviations from theoretical predictions can occur in the angular velocity and/or sense of rotation. The smaller the *S*, the greater the deviation and the more likely that antithetic rotation occurs. At constant *S*, deviations also occur as a result of the degree of coupling at the inclusion/matrix interface; antithetic rotation is enhanced by a slipping inclusion/matrix interface. If the sum of viscous-flow-driven rotation and pressure-gradient-driven rotation is positive, the rotation is synthetic, otherwise the rotation is antithetic.

If our experimental modelling is correct and applicable to nature, then:

1. One must be very careful when using porphyroclast vorticity to determine shear sense, because, as our experiments show, during bulk simple shear flow antithetic rotation is possible, and to significant amplitudes. Nevertheless, stair-stepping seems to be still reliable, at least when using pressure shadows similar to the ones observed in our experiments.
2. Small *S* and/or slipping inclusion/matrix interfaces can be an alternative explanation for the fact that many ductile shear zones are not dominated by the presence of rolling structures (as defined by Van den Driessche and Brun, 1987)—our experiments showed that there are stable positions parallel, or at a small angle (synthetic or antithetic), to the shear plane.

Acknowledgements

Experiments were performed in the Experimental Tectonics Laboratory of LATTEX, a research unit funded by PLURIANUAL (125/N/92). We thank José Antunes and Filipe Rosas for helpful discussions. The manuscript was improved by comments from R. Weijermars and D. Jiang.

References

Bretherton, F.P., 1962. The motion of rigid particles in a shear flow at low Reynolds number. Journal of Fluid Mechanics 14, 284–304.

Freeman, B., 1985. The motion of rigid ellipsoidal particles in slow flows. Tectonophysics 113, 163–183.

Ghosh, S.K., Ramberg, H., 1976. Reorientation of inclusions by combination of pure and simple shear. Tectonophysics 34, 1–70.

Ildefonse, B., Mancktelow, N.S., 1993. Deformation around rigid particles: the influence of slip at the particle/matrix interface. Tectonophysics 221, 345–359.

Jeffery, G.B., 1922. The motion of ellipsoidal particles immersed in a viscous fluid. Proceedings Royal Society of London, Ser. A 102, 161–179.

Marques, F.G., Cobbold, P.R., 1995. Development of highly non-cylindrical folds around rigid ellipsoidal inclusions in bulk simple shear: natural examples and experimental modelling. Journal of Structural Geology 17, 589–602.

Passchier, C.W., Simpson, C., 1986. Porphyroclast systems as kinematic indicators. Journal of Structural Geology 8, 831–843.

Van den Driessche, J., Brun, J.-P., 1987. Rolling structures at large shear strain. Journal of Structural Geology 9, 691–704.

Weijermars, R., 1986a. Flow behaviour and physical chemistry of bouncing putties and related polymers in view of tectonic laboratory applications. Tectonophysics 124, 325–358.

Weijermars, R., 1986b. Polydimethyloxane flow defined for experiments in fluid dynamics. Applied Physics Letters 48, 109–111.

Weijermars, R., 1986c. Finite strain of laminar flows can be visualized in SGM 36-polymer. Naturwissenschaften 73, 33.